Article

Current Biology

Allosteric modulation of a human odorant receptor

Graphical abstract

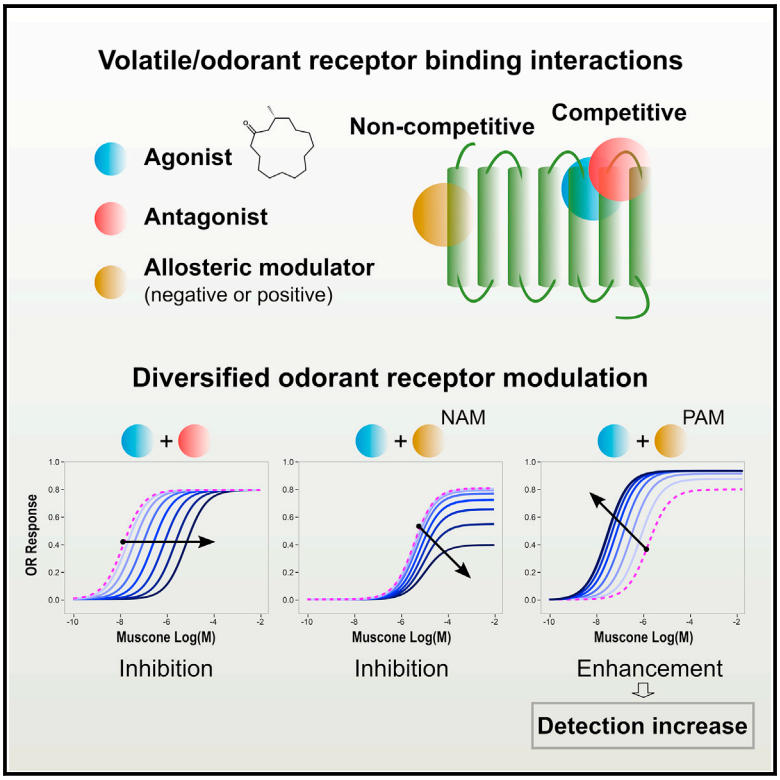

Authors

Casey Trimmer, Randy Arroyave, Christine Vuilleumier, ..., Christian Margot, Matthew E. Rogers, Patrick Pfister

Correspondence

patrick.pfister@firmenich.com

In brief

Widespread odorant receptor inhibition increases the sparsity of the olfactory code required to discriminate odorant mixtures. With the identification of positive allosteric modulators, Trimmer et al. show that a human musk receptor can also be enhanced by small volatile molecules, adding another layer to the encoding capacity of the olfactory system.

Highlights

- Musk receptor OR5AN1 appears to drive the detection threshold of its ligands
- Volatile, unsaturated aliphatic aldehydes can enhance the activity of OR5AN1
- Similar to other class A GPCRs, odorant receptors undergo allosteric modulation
- Allosteric modulation of ORs likely increases olfactory discrimination

Trimmer et al., 2023, Current Biology *33*, 1523–1534
April 24, 2023
https://doi.org/10.1016/j.cub.2023.03.016

CellPress

Current Biology

CellPress
OPEN ACCESS

Article

Allosteric modulation of a human odorant receptor

Casey Trimmer,[1] Randy Arroyave,[1] Christine Vuilleumier,[2] Lily Wu,[1] Aleksey Dumer,[1] Christie DeLaura,[1] Jehoon Kim,[1] Georgia M. Pierce,[1] Maria Borisovska,[1] Florian De Nanteuil,[2] Matthew Emberger,[1] Yakov Varganov,[1] Christian Margot,[2] Matthew E. Rogers,[1] and Patrick Pfister[1,3,*]

[1]Firmenich Inc., 250 Plainsboro Road, Plainsboro, NJ 08536, USA
[2]Firmenich SA, 7 Rue de la Bergère, Satigny 1242, Switzerland
[3]Lead contact
*Correspondence: patrick.pfister@firmenich.com
https://doi.org/10.1016/j.cub.2023.03.016

SUMMARY

Odor perception is first determined by how the myriad of environmental volatiles are detected at the periphery of the olfactory system. The combinatorial activation of dedicated odorant receptors generates enough encoding power for the discrimination of tens of thousands of odorants. Recent studies have revealed that odorant receptors undergo widespread inhibitory modulation of their activity when presented with mixtures of odorants, a property likely required to maintain discrimination and ensure sparsity of the code for complex mixtures. Here, we establish the role of human OR5AN1 in the detection of musks and identify distinct odorants capable of enhancing its activity in binary mixtures. Chemical and pharmacological characterization indicate that specific α-β unsaturated aliphatic aldehydes act as positive allosteric modulators. Sensory experiments show decreased odor detection threshold in humans, suggesting that allosteric modulation of odorant receptors is perceptually relevant and likely adds another layer of complexity to how odors are encoded in the peripheral olfactory system.

INTRODUCTION

Our sense of smell is the basis for the learned and innate behavioral responses required to navigate rich volatile chemical environments. At the periphery of the olfactory system, volatiles are detected by class A G-protein-coupled receptors (GPCRs) expressed in the olfactory sensory neurons (OSNs) of the nose. Each neuron expresses only one odorant receptor (OR) from a large gene repertoire, thus ensuring a unique identity for each neuronal cell.[1–4] Single odorants activate ORs with distinct receptive fields,[5–8] resulting in the combinatorial activation of a unique pattern of neurons that is translated into an olfactory percept.[9,10] However, our ORs most commonly encounter complex mixtures. Odorants compete to bind ORs, eliciting activation but also extensive and combinatorial inhibition via competitive antagonism.[11,12] This property has also been reported in the insect olfactory system, suggesting it represents a convergent solution for encoding the complexity of natural odors.[13] Indeed, these interactions have been shown to enable the combinatorial code to efficiently discriminate odor blends, contribute to functional OR diversification, and increase coding capacity by limiting neuronal activity saturation.[14–19]

Competitive OR inhibition, however, is not the only modulatory outcome possible in the presence of complex mixtures. In GPCRs, molecules can bind to allosteric sites distinct from those which bind an agonist and may modulate a receptor's response or lead to biased transduction cascade signaling.[20–22] Such allosteric modulation by small molecules has been reported for the heterodimeric sweet taste receptor with the identification of perceptually relevant enhancers.[23] In olfaction, enhancement has been reported in rodent OSNs,[18,24–27] suggesting that ORs may be responsible for this phenomenon and, similar to other class A GPCRs,[28–35] undergo non-competitive modulation. Furthermore, synergistic olfactory phenomena have also been reported in human psychophysical experiments with binary or complex, often food-related, odor mixtures,[36–38] although it is unclear whether they emerge from peripheral modulations, central processing, or both. Thus far, OR enhancement remains unreported in humans, and its putative effect on how we perceive quality, intensity, and sensitivity of odor blends is unknown. Positive modulation of OR activation and odor perception may lead to increased awareness of environmental danger (e.g., rotten food, poisonous compounds, or smoke) and would also be particularly relevant for pleasant-smelling compounds commonly used in perfumery. One such example is the musk family, a structurally diverse group of molecules with a powdery scent that provides the long-lasting base notes for many fragrances. Despite their long history of use, how their coveted scent is encoded by the olfactory system is not fully understood. Specific hyposmias, or the inability to smell certain musks, are common in the population[39–41] and can provide important clues to how their information in encoded.[42–45] For example, the inability to smell one musk can predict the inability to smell other, structurally unrelated musks,[46] indicating that some of these molecules may activate the same ORs and thereby share perceptual gateways despite differences in chemical structure. In support of this hypothesis, OR5AN1 was previously identified as a human musk receptor, which responds to structurally diverse musk compounds[47];

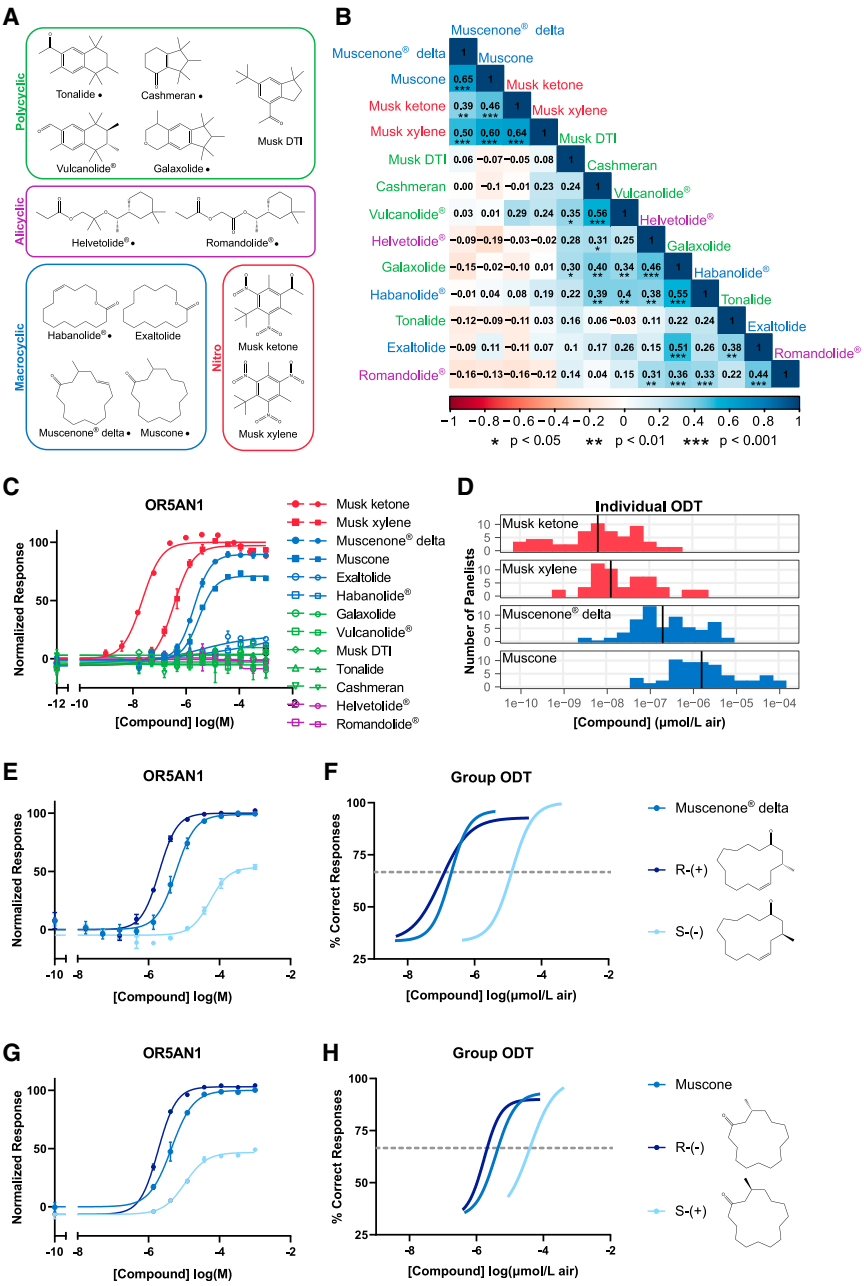

Figure 1. Correlation between OR5AN1 activation and human musk detection

(A) Chemical structure of 13 musk odors from four structural classes. ● indicates when the compound is a mixture of isomers.

(B) Correlation in individual odor detection thresholds (iODTs) for 13 musks for n > 54 participants. Label colors indicate musk structural classes. *p < 0.05, **p < 0.01, ***p < 0.001 for Spearman's rank correlation.

(C) Response of OR5AN1 to increasing doses of musk compounds, colored according to structural class. y axis represents homogeneous time resolved fluorescence (HTRF) values normalized to the response of OR5AN1 to musk ketone. Error bars are SEM over two replicates.

(D) Distribution of iODTs for four musks which activate OR5AN1 for n > 54 participants. Black bars indicate median iODT.

(E and G) Dose-response of OR5AN1 to muscenone delta, muscone, and their corresponding optical enantiomers. y axis represents HTRF values normalized to response to muscenone delta or muscone, respectively.

(F and H) Group odor detection threshold (gODT) for muscenone delta, muscone, and their corresponding enantiomers. Curves represent percent correct response for detection of increasing doses of compound for n > 30 participants. gODT is defined as the concentration at which the percent correct response is greater than 66%, represented by the dotted line.

See also Table S1.

RESULTS

Correlation between OR5AN1 activity and ODT

We extended previous work on specific anosmias to musks[46] to investigate whether human sensitivities to musk compounds were correlated. We determined individual ODTs (iODTs) for 13 musks falling into four different broad structural classes—polycyclic, macrocyclic, nitroaromatic derivative, and alicyclic (Figure 1A). We found that pairwise correlation in sensitivities for these musks did not cluster by structural class (Figure 1B) and identified three groups with highly correlated sensitivities: (1) muscone, muscenone delta, musk ketone, and musk xylene; (2) helvetolide, galaxolide, habanolide, exaltolide, and romandolide; and (3) cashmeran and vulcanolide. Group (1) includes a subset of macrocyclic ketones and nitroaromatic derivatives ("nitromusks"), two classes without any obvious common structural features, while the correlation matrix segregates macrocyclic ketones from the more closely related macrocyclic lactones. These data indicate that sensitivity to one member of a group significantly predicts sensitivity to the other group members independently of chemical similarity and suggest group members share part of their neuronal activity code.

however, we lack evidence directly relating activation of this OR to musk perception.

Here, we demonstrate that activation of OR5AN1 appears to drive odor detection threshold (ODT) for a group of chemically diverse musks and use this relationship to describe receptor-based enhancement in the human olfactory system. We identify compounds that increase the activity of OR5AN1's response to these musks, characterize the non-competitive molecular mechanism of this enhancement, and demonstrate that an enhancer decreases the ODT of muscenone and muscone in humans. Our results show that peripheral enhancement is receptor based, detectable, and may play a role in our ability to better discriminate odor blends.

Because members of group (1) have been previously shown to activate OR5AN1,[48] we tested OR5AN1's response to the panel of 13 musks and confirmed that OR5AN1 responded to all members of group 1 albeit with varying activity levels (Figure 1C). We found that the median iODT for muscenone delta, muscone, musk ketone, and musk xylene (Figure 1D) was rank-ordered according to OR5AN1 potency (a measure of affinity for the compound) and efficacy (a measure of activation strength) (see Table S1). For example, musk ketone had the lowest detection threshold and the lowest EC_{50} (highest potency) and muscone had the highest detection threshold and the highest EC_{50} (lowest potency) (Pearson correlation between iODT and EC_{50}, $r = 0.87$). In addition, musk ketone and musk xylene were full agonists, with similar iODTs, while muscenone delta and muscone were partial agonists with iODTs that correspond to the efficacy of their response (Pearson correlation between iODT and maximal efficacy of response, $r = -0.91$).

To further probe the relationship between receptor activity and human sensitivity, we examined the correlation between OR5AN1's response to the optical isomers of the two macrocyclic ketones and their ODTs. We collected group ODTs (gODTs), a fast and reliable method to efficiently measure odor detection probability in a group of subjects. The gODTs of muscenone delta and its R (+) enantiomer are two orders of magnitude lower than the S (−) enantiomer, indicating that the R enantiomer likely drives the low gODT of racemic muscenone. In line with these psychophysical observations, the EC_{50} of OR5AN1's response to the racemic mixture and (R)-(+)-muscenone is an order of magnitude lower than that of (S)-(−)-muscenone (Figures 1E and 1F) (Pearson correlation between gODT and EC_{50}, $r = 0.99$). Similarly, muscone and its R (−) enantiomer have gODTs and EC_{50}'s that are an order of magnitude lower than those of the S (+) enantiomer (Figures 1G and 1H) (Pearson correlation between gODT and EC_{50}, $r = 0.97$). For both compounds and regardless of optical activity (i.e., rotary polarization), OR5AN1 displays strong enantioselectivity for the R conformer, consistent with previous reports.[47,48] Taken together, the data indicate that OR5AN1 activity may encode muscone, muscenone delta, musk ketone, and musk xylene detection and appears to drive the observed ODTs. Overall, the ODTs of these musks were inversely correlated with their potency and efficacy on the receptor.

Enhancement of OR5AN1 activity by aliphatic unsaturated aldehydes

To provide additional support that OR5AN1 activation drives the perception of these musks, we hypothesized that altering the receptor response would have a corresponding effect on sensitivity in human subjects. We examined the ability of 780 structurally diverse compounds to alter the activation of OR5AN1 in the presence of a low activating concentration (EC_{20}) of muscenone delta (Figure 2A). Roughly 150 compounds decreased the response of OR5AN1 by greater than three standard deviations from the EC_{20} baseline, in line with previous results demonstrating the prevalence of inhibition at the periphery of the olfactory system (Figure 2A, red). In addition, we also observed that 24 compounds increased activation (Figure 2A, green), including known activators (i.e., macrocyclic ketones and nitromusks), and compounds that were weak or non-agonists and thus had the potential to act as enhancers. In subsequent dose-response experiments, five compounds increased the potency of OR5AN1's response to muscenone delta between 9- and 19-fold ((2E,6Z)-2,6-nonadienal and (Z)-2-nonenal, respectively) when present at a concentration of 250 μM (Figures 2B–2F). At this concentration, these compounds bound the receptor and behaved as partial agonists as evidenced by their low but apparent activation of OR5AN1. Note, we did not observe the decrease in OR activation we would expect if these molecules were competing for the same binding site as muscenone delta, indicating that these interactions were likely non-competitive. These five compounds had similar structures: long chain (C9–13), unbranched aldehydes with an unsaturation at the α-β position; in contrast, similar aldehydes without the α-β double bond did not alter the response of OR5AN1 to muscenone delta (Figures 2B–2F).

We next sourced 111 compounds with varied chain length, functional group, saturation, and branching to probe the structure-activity relationship (SAR) of OR5AN1 enhancers. Eight compounds shifted the EC_{50} of OR5AN1's response to muscenone delta by more than 7-fold, a difference that was sufficient to observe a change in the gODT of muscenone delta enantiomers (see Figures 1E and 1F). These included four additional compounds not identified in the original screen: (Z)-2-decenal, (2E,6Z)-2,6-nonadienal, (E)-2-6,7-dimethyl-2,6-octadienal, and (E)-2-undecenal (Figure 3A). Aldehydes were the only functional group that effectively enhanced the potency of OR5AN1's response to its agonist. Unsaturation at the α-β position was further required, while branching with methyl groups was tolerated. For example, 9- and 13-carbon alcohols or acids that were unsaturated at the α-β position did not significantly alter the EC_{50} of OR5AN1's response to muscenone delta (Figures 3B and 3C). Similarly, saturated aldehydes, or compounds lacking a double bond in the α-β position, lost the ability to enhance. OR5AN1 efficacy was also increased by the presence of enhancers. The greatest shift in efficacy was elicited by (E)-2-undecenal, which increased efficacy by 1.3-fold. Overall, the results revealed that the chemical requirements leading to OR5AN1 enhancement are aliphatic aldehydes between 8 and 13 carbons in length and unsaturated at the α-β position.

Non-competitive OR5AN1 binding interactions

The identification of compounds with enhancing properties strongly suggested non-competitive binding interactions may occur. To test this hypothesis, we examined the response of OR5AN1 to muscenone delta in the presence of a series of enhancer concentrations, focusing on the nine enhancers identified in Figure 3, in addition to two negative controls: nonanal, fully saturated and (Z)-4-dodecenal, unsaturated in γ-δ position (Figure S1). Enhancement was dose dependent, requiring a minimum concentration of modulator, starting at 22 μM according to our experimental design, and reached a plateau between 67 and 200 μM for most compounds, probably reflecting saturation of the enhancer binding site (see Figures S1A–S1D and S1I). Other modulators showed a decrease in enhancement at higher modulator concentrations (see Figures S1E–S1H), potentially indicating that higher concentrations of enhancer were insoluble or toxic in our cell assay conditions though we did not observe any evidence supporting this. Alternatively, the modulator may

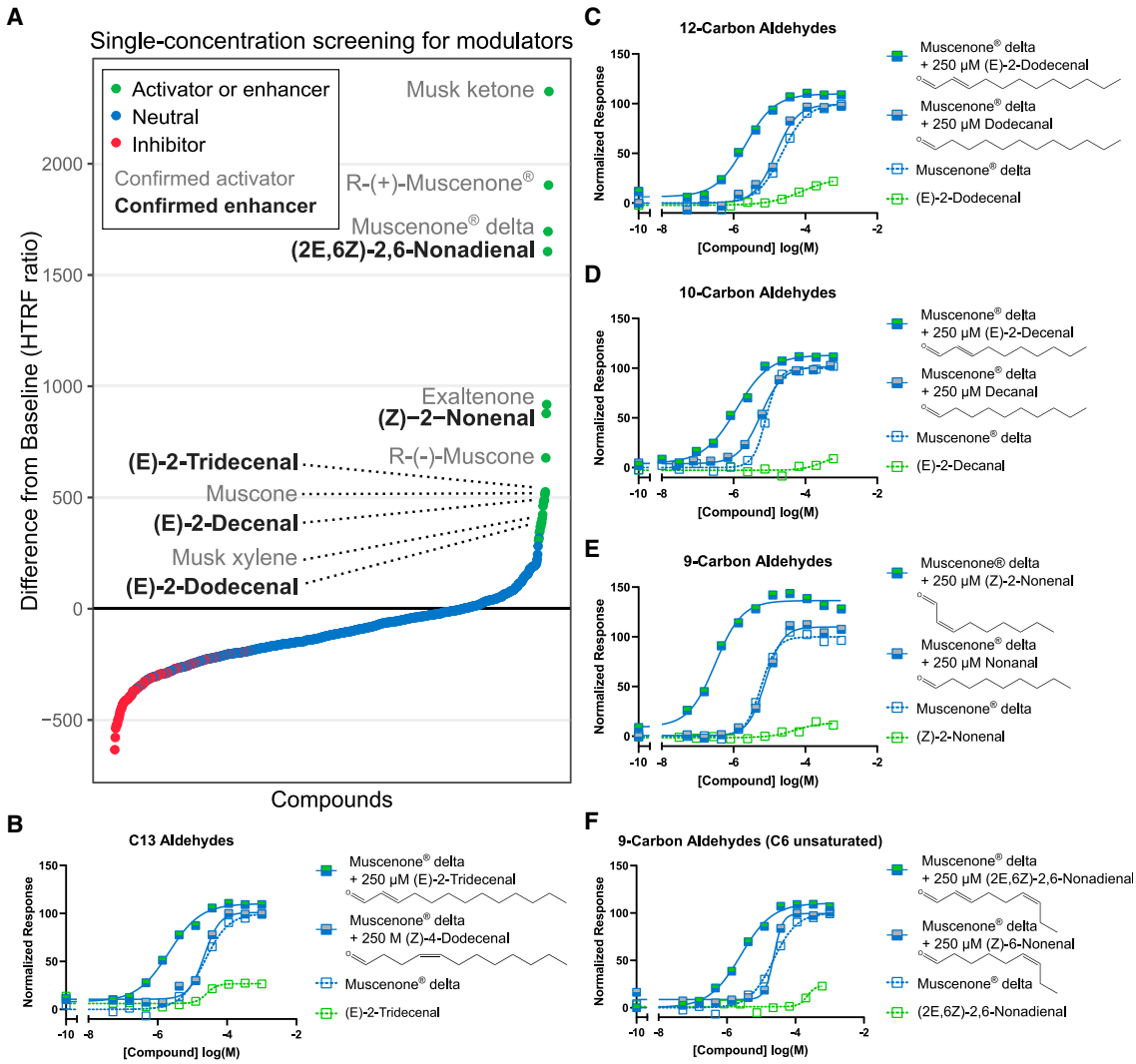

Figure 2. Identification of compounds which enhance OR5AN1 activation

(A) Single-concentration screening for ability of 780 compounds (at 250 μM) to increase the response of OR5AN1 to muscenone delta (at 15 μM). Compounds are ordered according to difference in HTRF values compared with baseline (response to 15 μM muscenone delta). Compounds increase (>3 standard deviations above baseline, green), decrease (>3 standard deviations below baseline, red), or had no effect (less than 3 standard deviations from baseline) on the response of OR5AN1 to muscenone delta. Green compounds include activators (plain text) and enhancers (bold text), confirmed in dose-response experiments.

(B–F) Dose-response of OR5AN1 to muscenone delta (blue boxes) in the presence of enhancers identified in the screen (partially open boxes) and structurally related compounds (gray) or enhancer alone (open boxes). y axis represents HTRF values normalized to the response of OR5AN1 to muscenone delta.

See also Figures S1–S3 and Tables S2 and S3.

favor distinct ternary complex conformations at different concentrations, potentially leading to bimodal effects.

The dose-response curves were fitted to the operational allosteric equation derived from the ternary complex model. This model is typically used to characterize allosteric modulation and describes the magnitude of change in potency (α cooperativity factor) and efficacy (β cooperativity factor), in addition to affinity (K_B) and intrinsic efficacy (T_B, fraction of maximum response to agonist) of the enhancer[20,21] (see Tables S2 and S3). The α and β cooperativity values are greater than 1 for all enhancers, consistent with positive allosteric modulation, and close to 1 for the negative controls, consistent with a lack of modulation (see Figure S1 insets and Tables S2 and S3). Enhancer potency ranged from 10 to 100 μM, and some compounds were able to elicit receptor activity on their own without the presence of ligand ($T_B > 0$).

The cooperativity constants from the operational allosteric model describe the interaction between each agonist/modulator pair and the receptor and can differ for other agonists. This phenomenon is called allosteric probe dependence and reflects the reciprocal modulation that can occur when two compounds contact the receptor simultaneously.[49] We investigated probe dependence for OR5AN1 enhancement by examining the ability of (Z)-2-nonenal, (E)-2-tridecenal, and two negative controls to enhance the response of OR5AN1 to four ligands: muscenone delta, muscone, musk ketone, and musk xylene. These

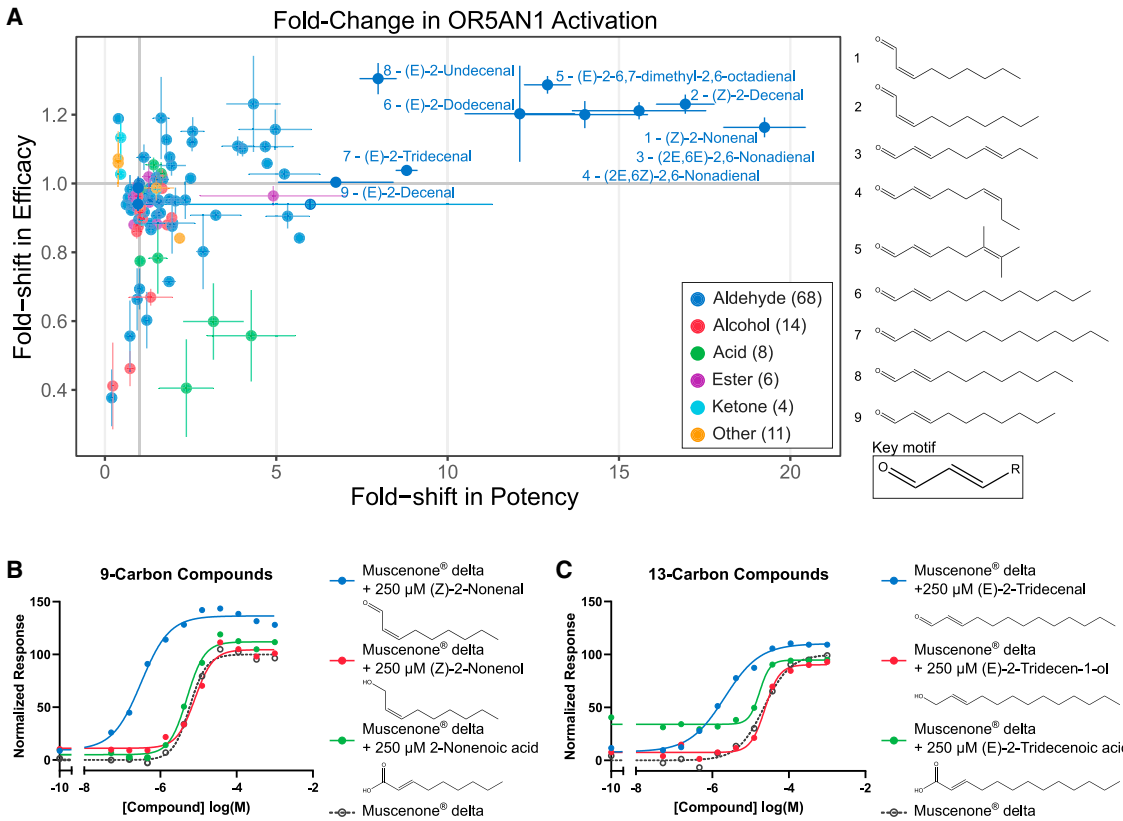

Figure 3. Structure-activity analysis of requirement for OR5AN1 enhancement

(A) Fold-change in potency and efficacy of OR5AN1 response to muscenone delta in the presence of 250 µM of a panel of 111 aldehydes, alcohols, acids, esters, and ketones. Enhancers which shift EC_{50} greater than 7-fold shared a similar structure: aliphatic aldehydes unsaturated at the α-β position (key motif boxed). Points represent mean response ± SEM (n ranged from 1 to 19 experiments).

(B and C) Dose-response of OR5AN1 to muscenone delta (open circle) in the presence of two aldehydic enhancers (blue) and their alcohol (red) and carboxylic acid (green) related structures. y axis represents HTRF values normalized to the response of OR5AN1 to muscenone delta.

See also Figures S1–S3 and Tables S2 and S3.

enhancers spanned the carbon chain length required for enhancement (9 and 13 carbons) and the magnitude of enhancement (19- and 9-fold increase in potency) (Figure S2; Tables S2 and S3). (Z)-2-nonenal increased either the affinity (α ranged from 9.9 to 69.6) or the efficacy (β ranged from 0.8 to 3.1), sometimes both, of the response of OR5AN1 to all ligands (Figures S2A, S2E, S2I, and S2M). Interestingly, β is greatest for the effect of (Z)-2-nonenal on muscone response (β = 3.1), most likely because its partial response in the absence of enhancer allows a larger response window following receptor modulation. (E)-2-tridecenal also had a positive, but smaller, effect on the affinity of OR5AN1's response to muscone, musk ketone, and musk xylene (α ranged from 4.6 to 16.7), and relatively little effect on efficacy (β ranged from 0.7 to 0.9) (Figures S2C, S2G, S2K, and S2O). In addition, we analyzed the potential reciprocal modulatory effect of the orthosteric ligand on the two enhancers and observed that both their apparent affinity was virtually unaffected. Within the dynamic concentration range of the agonist, (Z)-2-nonenal and (E)-2-tridecenal potencies only minimally increased as a function of muscenone delta's concentration (Figure S3). These results indicate both (Z)-2-nonenal and (E)-2-tridecenal enhanced the response of OR5AN1 to different agonists to varying degrees, reflecting the probe dependence commonly found in allostery.[49]

We next searched for potential negative modulators of OR5AN1. We identified a polycyclic musk, galaxolide, able to inhibit OR5AN1 activation and characterized its ability to decrease the response to four ligands (Figure S4; Tables S2 and S3). Galaxolide decreased the potency but also the maximum efficacy of OR5AN1 to muscenone delta, muscone, and musk xylene by greater than 40% when present at 600 µM and only minimally for musk ketone. In a strictly competitive interaction, maximum efficacy is typically achieved by the agonist as increasing concentrations eventually outcompete the antagonist, preventing its binding. Here, agonists were unable to outcompete galaxolide even at high concentrations, while still eliciting a complete, albeit weaker dose-response curve. This is characteristic of non-competitive inhibition where the two compounds bind the receptor simultaneously under the assumptions of the operational allosteric model. The different degrees of inhibition elicited by galaxolide are further evidence for allosteric probe-dependency. Collectively, these results show that OR5AN1 is susceptible to both positive and negative allosteric modulation.

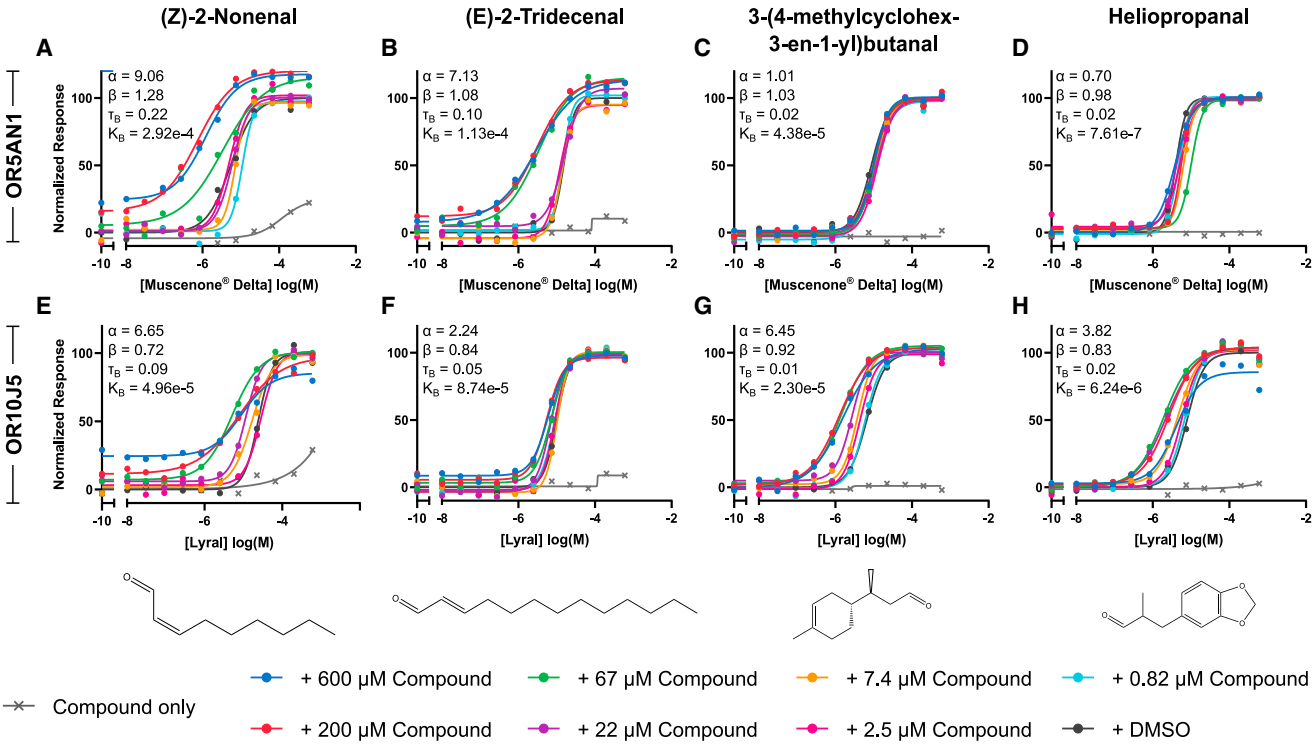

Figure 4. Pharmacological analysis of receptor-specificity of enhancement

(A–D) Dose response of OR5AN1 to muscenone delta and (E–H) OR10J5 to lyral in the presence of DMSO or 7 concentrations of (Z)-2-nonenal, (E)-2-tridecenal, 3-(4-methylcyclohex-3-en-1-yl)butanal, and heliopropanal. Response to compound alone is also shown. y axis is HTRF values normalized to the response of OR5AN1 or OR10J5 to agonist alone in the presence of DMSO. Inset shows α and β (cooperativity factors governing changes in potency and efficacy, respectively), TB (efficacy of modulator), and KB (affinity of modulator in μM) calculated from fitting data to the operational allosteric model.
See also Figure S4 and Tables S2 and S3.

Receptor-specific enhancement

We thus asked whether allosteric modulation was unique and specific to OR5AN1. We first examined a closely related receptor, Olfr1440, the mouse ortholog of OR5AN1, which also responds to muscenone delta.[47] Both (Z)-2-nonenal and (E)-2-tridecenal moderately activated Olfr1440, as observed for OR5AN1, but did not strongly enhance the response potency or efficacy of Olfr1440 to muscenone delta ($\alpha < 3.2$ and $\beta < 0.97$) (Figure S4; Tables S2 and S3). These results indicate that Olfr1440 binds both compounds, but significant enhancement was observed only with the human receptor. Given that the effect of the enhancers on Olfr1440 and OR5AN1 were not the same while their agonist-binding pockets are orthologous, enhancement seems specific and unlikely to be the result of a physical interaction between musk and enhancer.

We next examined the effect of (Z)-2-nonenal and (E)-2-tridecenal on the activation of a human lyral receptor OR10J5, only distantly related to OR5AN1 with ~42% amino acid identity (Figure 4; Tables S2 and S3). Following the same approach as in Figure 2, we identified two compounds—3-(4-methylcyclohex-3-en-1-yl)butanal and heliopropanal—that enhanced the potency of OR10J5's response to lyral ($\alpha = 6.4$ and 3.8, respectively), had minimal effect on efficacy ($\beta < 0.93$), and did not strongly activate the receptor by themselves ($T_B < 0.02$) (Figures 4G and 4H). These compounds had no effect on the response of OR5AN1 to muscenone delta ($\alpha = 1$ and 0.7, respectively, and $\beta \sim 1$, Figures 4C and 4D). In contrast, OR10J5 responded weakly to both (Z)-2-nonenal and (E)-2-tridecenal ($T_B = 0.09$ and 0.05, respectively) indicating that binding of the receptor, and both compounds, increased the potency of OR10J5's response to lyral ($\alpha = 6.7$ and 2.2, respectively) (Figures 4E and 4F). However, (E)-2-tridecenal's effect on OR5AN1 was more pronounced ($\alpha = 7.1$). Furthermore, although the potency shift was greater for OR10J5 than OR5AN1, (Z)-2-nonenal decreased the efficacy of the response of OR10J5 to lyral ($\beta = 0.7$), indicating the (Z)-2-nonenal is not a straightforward positive modulator for OR10J5. Similarly, heliopropanal reduced the efficacy of the OR10J5 response to lyral but only at the highest concentration tested (600 μM). Given the presumed differences in the orthosteric binding sites of these receptors, their ability to both bind (Z)-2-nonenal and (E)-2-tridecenal provides further evidence these compounds are binding a site distinct from that of the agonist. Overall, the data support that enhancement can be receptor specific.

Mutational analysis of enhancement and activation response properties

To explore the receptor-based nature of enhancement, we sought to identify amino acid residues involved in the modulation of OR5AN1 activity. We generated single point mutations

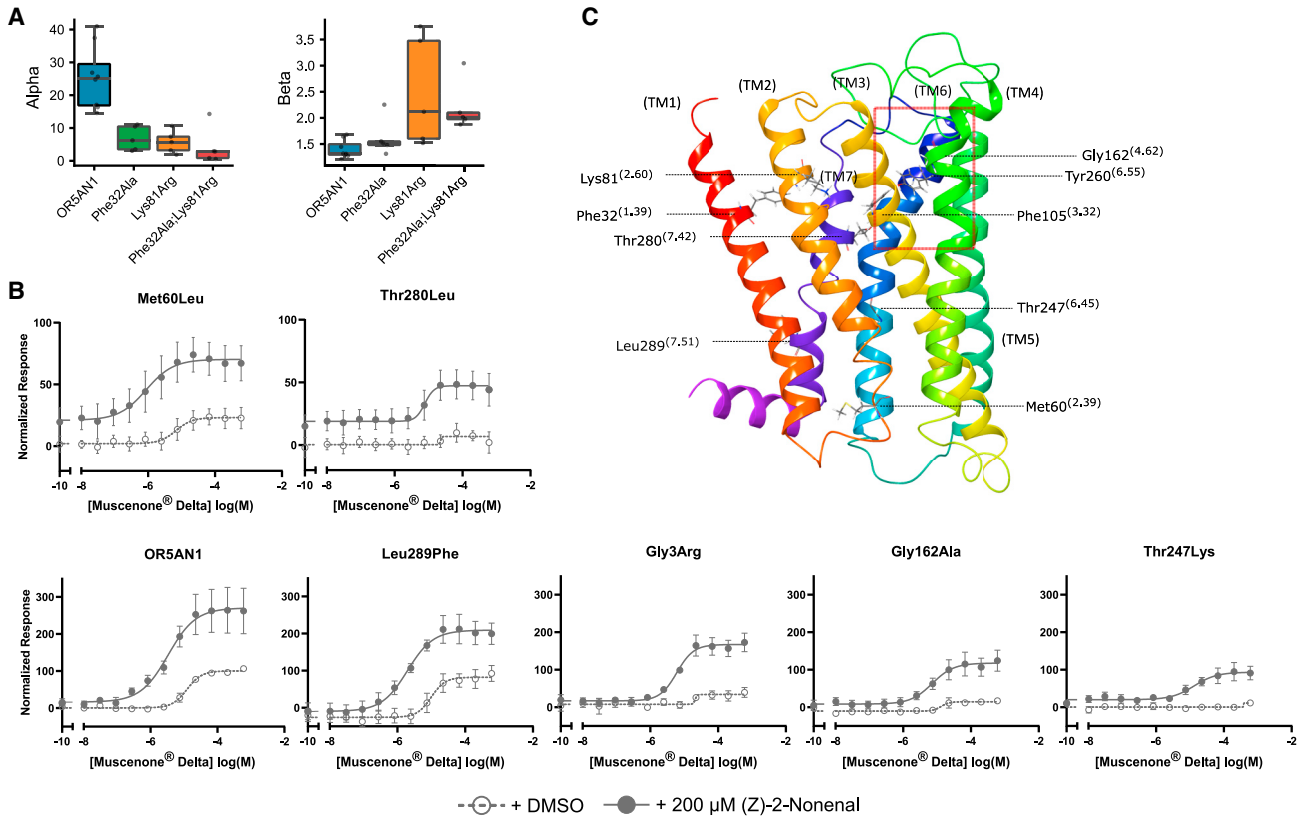

Figure 5. Identification of residues important for enhancement of OR5AN1 activation

(A) Cooperativity factors α and β (governing changes in potency and efficacy, respectively) calculated from fitting the operational allosteric model to the response of OR5AN1 to muscenone delta in the presence of DMSO or seven concentrations of (Z)-2-nonenal. Results represent median α and β ± SEM for wild-type OR5AN1 and mutations at residues 32 and 81 singly and in combination (n = 5 experiments).

(B) Response of OR5AN1 mutated at residues 60 and 280 and five population variants to muscenone delta in the presence of DMSO or 200 μM (Z)-2-nonenal. y axis is HTRF values normalized to the response of OR5AN1 to muscenone delta alone in the presence of DMSO. Points represent mean response ± SEM (n = 4 experiments).

(C) 3D model of OR5AN1 showing the orthosteric binding pocket (red box) and the location of residues identified to be involved in ligand binding (Phe105 and Tyr260),[50] the residues affecting enhancement (Phe32 and Lys81) or activation (Met60 and Thr280), and three naturally occurring mutations (Leu289, Gly162, and Thr247). Gly3 is located in the N-terminal of the receptor and falls outside of the model.

See also Figures S5 and S6 and Tables S2 and S3.

throughout the receptor and examined their effects on both activation and enhancement. To disentangle mutations exerting conformational changes broadly affecting the receptor's properties from those potentially involved in conferring allosteric properties to the receptor, we restricted our analysis to mutants that affected enhancement only. Residues Phe32 and Lys81, when mutated to Ala and Arg, respectively, did not significantly alter the response of the receptor to muscenone delta (fold-change in potency 1.1 and 1.4, respectively), however they decreased (Z)-2-nonenal's ability to enhance OR5AN1 activation potency by roughly half when present at 200 μM. The median potency cooperativity factor α decreased from 25.2 for the wild-type sequence to 5.9 for both mutants ($p = 4.6e{-}5$, Mann-Whitney U test) and even further to 2.9 when both residues are mutated in combination ($p = 0.13$ between single- and double mutants, Mann-Whitney U test), while the efficacy cooperativity factor β was slightly increased relative to wild type (median wild type $\beta = 1.32$, median mutant $\beta = 1.98$, $p = 0.004$, Mann-Whitney U test; Figures 5A and S5A; Tables S2 and S3).

Following the procedure in Ahmed et al.,[50] we built a homology model of OR5AN1, based on the M2 muscarinic acetylcholine receptor (Figure 5C). The authors showed that residues Phe105 and Tyr260, located in transmembrane domains TM3 and TM6, respectively, are involved in the binding of musk ligands. Residues Phe32 and Lys81 are located in TM1 and TM2, a region that lies outside the orthosteric binding pocket and described as a prototypical allosteric site of class A GPCRs.[51] We further turned to docking analyses to gain more insight into the potential role of these residues in stabilizing an enhancer. Because our most effective enhancers were α-β unsaturated aldehydes and aldehydes are known to interact with lysine side chains via their carbonyl group,[52] we anchored (Z)-2-nonenal and nonanal on Lys81 through an imposed hydrogen bond and evaluated their position in the putative binding area. Under these constraints, (Z)-2-nonenal closely associates with the hydrophobic side chains of residues around Phe32, including Val79 and Leu83. In contrast, the tail of nonanal did not establish contact with these hydrophobic residues (Figure S6). Although mutating

Lys81 to arginine did not eliminate enhancement (α = 5.9), we postulate that it may instead establish a strong polar network with the carbonyl group of (Z)-2-nonenal. In combination with the loss of hydrophobic contact with Phe32, enhancement is reduced even more (α = 2.9). In line with this, mutation of either Val79 or Leu83 to alanine or threonine decreased the receptor response to muscenone delta (data not shown). Assuming that Val79 and Leu83 may be key contact residues that commonly exist in class A GPCRs, this could explain how (Z)-2-nonenal, but not nonanal, modulates OR5AN1 function. The estimated binding free energies indicated that both binding modes of (Z)-2-nonenal and nonanal are stable. Nonanal seems thus equally able to bind OR5AN1 but elicits no activation or modulation, perhaps due to the lack of contact with the hydrophobic motif near Phe32. Although our docking results support the possibility that the binding of (Z)-2-nonenal may be mediated by polar and hydrophobic interactions with Lys81 and Phe32, respectively, they represent just one possibility for a potential enhancer binding site. The binding mode and a full characterization of allosteric binding events remains to be explored.

Finally, we also identified two mutations, residues Met60Leu and Thr280Leu, with a much-decreased response to muscenone delta. However, they retained their ability to be enhanced in a dose-dependent manner (Figures 5B and S5B; Tables S2 and S3). The ability of the enhancer to rescue the response of a seemingly non-functional variant of the receptor led us to examine the effect of enhancement on naturally occurring functional variants of OR5AN1. We assessed the effect of (Z)-2-nonenal on five OR5AN1 alleles, two of which appeared to be hypofunctional and one non-functional. We observed an increase in response in the presence of the enhancer for all five alleles tested, comparable to that of the unmodulated reference receptor response, even in the case of the non-functional allele Thr247Lys (Figures 5B and S5C; Tables S2 and S3). Therefore, minor changes, even of a single nucleotide, appear to affect not only how the receptor responds to individual compounds but also to mixtures, by altering its ability to be modulated.

ODT decrease in the presence of an enhancer

Given the correlation between the potency of OR5AN1's response to its ligands and observed musk sensitivities in human subjects (Figure 1), we hypothesized that compounds that decrease the EC_{50} of musk agonists *in vitro* would have a corresponding effect on ODT *in vivo*. To this end, we examined the gODT for muscenone delta in the presence of (E)-2-tridecenal and its corresponding negative control (Z)-4-dodecenal, as well as the gODT for muscenone delta and the pure muscone laevo enantiomer (R-(−)-muscone) in the presence of a more potent enhancer (Z)-2-nonenal and its corresponding negative control nonanal, by using an adaptation of the ASTM E-679 method (2008) (Figure 6). We employed a forced-choice detection method with varying musk concentrations in the presence of a constant concentration of enhancer or control volatile compound. The concentrations of enhancer and control compounds were selected to be iso-intense (see STAR Methods). Detection probabilities were modeled as a function of the musk concentration by fitting a logistic equation with three parameters: asymptotic probability of detection with increasing concentration (max P_d), concentration at which probability of detection equals max P_d/2 (θ), and Hill coefficient for the fitted curve (Figure 6). Because θ comparisons are meaningful only for curves with a similar max P_d, these comparisons were performed whenever max P_d of enhancer vs. control condition were not significantly different (Figure 6L). We then performed bootstrap tests to calculate confidence intervals of these parameters. In addition, for each bootstrapped curve, we calculated the mean detection probability (mean P_d) and its confidence intervals by averaging detection probabilities at each ligand concentration. The advantage of mean P_d as an outcome variable is that it is a summary measure of detection probabilities over the actual concentration range examined in the study rather than the extrapolated asymptote. Because it is based on more data, it is also a more stable estimate than max P_d. Randomization tests were used to statistically compare mean P_d, max P_d, and Hill coefficients for each enhancer-control pair.

There was no evidence that the detection of muscenone delta changes in the presence of (E)-2-tridecenal relative to (Z)-4-dodecenal as all parameters were not significantly different (Figures 6A–6D). Max P_d and mean P_d with (Z)-2-nonenal were, however, significantly different from nonanal (max P_d = 1.00 vs. 0.54, p = 0.016; and mean P_d = 0.46 vs. 0.34, p = 0.0009 for (Z)-2-nonenal vs. nonanal, respectively; Figures 6E–6G). Similarly, mean P_d and θ of muscone with (Z)-2-nonenal were significantly different from nonanal (mean P_d = 0.37 vs. 0.26, p = 0.007; and θ = 0.001 M vs. 0.013 M, p = 0.004, for (Z)-2-nonenal vs. nonanal, respectively; Figures 6I, 6K, and 6L), while max P_d was not (Figure 6J). The Hill coefficients were not significantly different in either condition (data not shown). These results show that the application of a compound which changes receptor potency and/or efficacy can translate to alterations in detection sensitivity.

DISCUSSION

We examined the perceptual relevance of a human OR involved in the detection of a subset of musk compounds and used it to characterize a phenomenon largely unexplored at the receptor level: positive OR modulation. We showed that OR5AN1 activation likely drives human sensitivity to nitromusks and macrocyclic ketones, but not macrocyclic lactones, and examined how manipulation of its activity affected perception. We first showed how ODT for a distinct subclass of musks directly correlated with OR5AN1 activity, and similarly how the detection of enantiomers (with identical volatilities and likely comparable vapor pressures[53]) correlated with OR5AN1 enantioselectivity. We then characterized the potential for volatile compounds to enhance OR5AN1's response to musks and, following a robust SAR-based screening campaign, identified multiple enhancers. Several lines of evidence indicate that these compounds are positive allosteric modulators (PAMs). First, the enhancers did not compete with agonists for the orthosteric site in dose-response experiments, even for compounds with apparent dose-dependent activity, as inhibition would have been the expected outcome. Instead, it appears that the partial activity observed is due to allosteric agonism. Second, enhancement was receptor specific and exhibited probe dependence (i.e., the modulation effect is co-dependent on the agonist), an expected property of PAMs. Finally, the operational allosteric

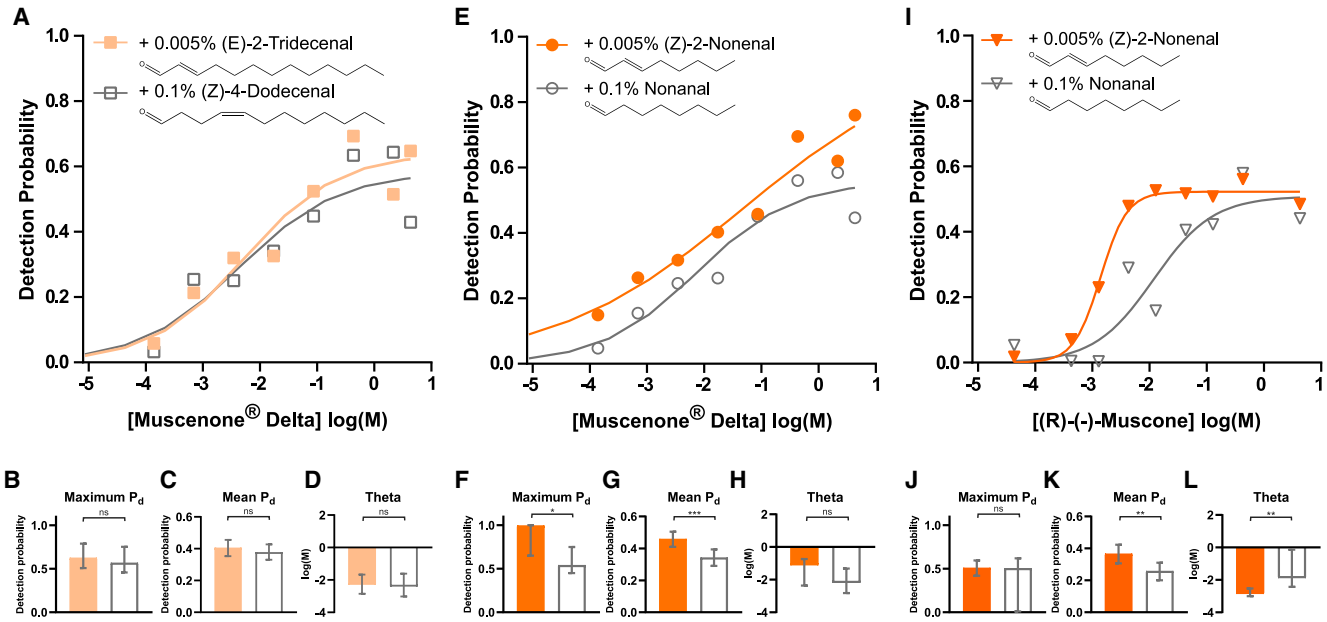

Figure 6. Enhancement of musk detection

(A) Detection curves for muscenone delta in the presence of (E)-2-tridecenal or control (Z)-4-dodecenal.

(E) Detection curves for muscenone delta in the presence of (Z)-2-nonenal or nonanal.

(I) Detection curve for R-(−)-muscone in the presence of (Z)-2-nonenal or nonanal.

(B–D, F–H, and J–L) In each experiment detection probability curves were statistically compared on four parameters: max P_d, asymptotic probability of detection with increasing concentration (B, F, and J), mean P_d, mean probability of detection across concentrations tested (C, G, and K), θ, a logarithm (base 10) of molar concentration at which the fitted curve reaches max $P_d/2$ (D, H, and L), and Hill coefficients (not shown). Bars are 95% confidence intervals calculated by bootstrapping the fitting of the detection curve; p values, *$p < 0.05$; **$p < 0.01$.

model was a good fit for our data (median RMSE = 0.03); in fact, competitive models cannot encompass positive modulation.

One of the best enhancers—(Z)-2-nonenal—decreased the detection threshold of muscenone delta and muscone in sensory experiments compared with non-enhancers compounds, supporting a direct role for OR5AN1 in the detection of macrocyclic ketones. These data extend previous findings linking genetic variation in OR5AN1 to changes in musk detection[54] and add to the growing list of ORs that can be successfully tied to a perceptual feature.[42–44,55–57] Considering studies demonstrating the most sensitive OR for an odorant drives its detection threshold in mice,[47,58] OR5AN1 may be the most sensitive receptor for nitromusks and macrocyclic ketones in humans.

Our results show that ORs share fundamental pharmacological properties with canonical class A GPCRs (e.g., muscarinic, opioid, cannabinoid, or serotonin receptors) in that interaction with small molecules may modulate receptor activity. All 10 compounds able to enhance the response of OR5AN1 to its activating musks were α-β unsaturated aliphatic aldehydes. The reason for this restricted SAR, compared with the breadth of SAR observed for competitive inhibition,[14–19] may be that volatile allosteric modulators of ORs are simply rare due to a more constrained allosteric binding pocket. Such restricted receptive fields for allosteric ligands compared with orthosteric ones is a feature observed for other GPCRs and exploited by drug design approaches for increased targeting specificity.[22] The ability of (Z)-2-nonenal to enhance the activation of two ORs with different ligand specificities may however indicate some degree of conservation of the allosteric binding site even in significantly diverged ORs.[59] The full extent to which these findings can be extended to other ORs, and the prevalence of OR enhancement, remain to be explored.

OSN enhancement recorded at the periphery has been reported to reach the pre-synaptic glomerular regions of the olfactory bulb,[16] supporting that peripheral enhancement can modulate central activity. However, how much of a shift in receptor activation is necessary for perceptual relevance is unknown. Although we tested enhancers that caused a ~19- and ~9-fold shift in potency, only the stronger enhancer identified showed a statistically significant decrease in the detection threshold of muscenone delta and muscone. This may reflect the fact that a certain threshold of receptor activity enhancement must be achieved to realize a perceivable difference. In addition, because muscone is a partial agonist of OR5AN1 and exhibited the largest sensitivity shift, the results further suggest that enhancement of the efficacy may be more effective at enhancing ODT compared with solely potency. Identifying a range of allosteric modulators, including those with much stronger positive or negative effects and better affinities compared with the ones described here, would allow to test these hypotheses further and more precisely determine how receptor modulation relates to detection sensitivity at peri-threshold concentrations.

The identification of residues involved in the binding properties of OR5AN1 revealed how a single point mutation can affect its response profile to distinct ligands and mixtures thereof. Two mutants, at positions Phe32 and Lys81, generated a reduction

in the ability of (Z)-2-nonenal to enhance the receptor, apparently without affecting the response to the musk agonist. Both mutants and the corresponding double mutant, however, only affected the potency. The mutated residues therefore did not modify the receptor by limiting its transduction efficacy, but presumably by decreasing its affinity to the modulator and/or the agonist, underscoring how receptor composition may dynamically impact GPCR conformation and downstream activation pathways.[60] For example, PAMs have been shown to increase the residence time of the agonist in class C GPCRs.[61] In contrast, two additional mutants, at positions Met60 and Thr280, lost their ability to respond to muscenone delta alone, a response that could be partially rescued in the presence of the enhancer. Similarly, the five OR5AN1 alleles tested exhibited functional variation upon binding to the ligand—spanning fully-, hypo-, and non-functional variants—but conserved enhancement property that led to increased responses to the binary mixture for all alleles, including the three poor responders. This latter result suggests that hypo-functional alleles that may be responsible for weak detection or even specific anosmia, may in fine be perceptually relevant for complex mixtures if synergistic interactions between volatiles occur.

Cell-based studies of OR activation commonly focus on individual odorants, leaving more complex receptor interactions hidden. However, simple binary mixtures can reveal the breadth of OR behavior, including competitive inhibition and allosteric positive or negative modulation uncovered here. While inhibition appears to be a prominent part of the olfactory code[16–19]; enhancement seems rarer in the mouse olfactory epithelium.[18] We nonetheless identified enhancers for two human ORs and showed one of them to elicit perceivable sensory benefit in detecting muscenone delta and muscone laevo. It appears that enhancers exhibit a combinatorial binding logic, typical of how volatiles interact with OSNs at the periphery. Compared with competitive inhibition however, allosteric modulation generates a far richer diversity of pharmacological outcome,[21] a property that may be required to differentiate very similar odorant mixtures. Despite the many questions that remain, these findings suggest that OR enhancement represents a new paradigm to encode the myriad of volatiles we encounter every day and thus adds another layer of complexity to how our noses process odors.

STAR★METHODS

Detailed methods are provided in the online version of this paper and include the following:

- KEY RESOURCES TABLE
- RESOURCE AVAILABILITY
  - Lead contact
  - Materials availability
  - Data and code availability
- EXPERIMENTAL MODEL AND SUBJECT DETAILS
  - Human Subjects
- METHOD DETAILS
  - Odor detection thresholds determination
  - Homogeneous time resolved fluorescence (HTRF) assay and high-throughput screening
  - Allosteric modulation parameter calculations
  - Psychophysical assessment of enhancement
  - Homology modeling and docking of OR5AN1
- QUANTIFICATION AND STATISTICAL ANALYSIS

SUPPLEMENTAL INFORMATION

Supplemental information can be found online at https://doi.org/10.1016/j.cub.2023.03.016.

ACKNOWLEDGMENTS

This work was fully funded internally by Firmenich. We would like to thank members of the R&D division for their contributions, in particular G. Servant, B.C. Smith, and D. Shcherbakov for comments on the manuscript; J. Pika and D. Hossain for compound analysis and management; and I. Cayeux, N. Freiburghaus, and P.-A. Rebetez for technical support.

AUTHOR CONTRIBUTIONS

Conceptualization, C.T., M.E.R., and P.P.; methodology and investigation, C.T., R.A., C.V., L.W., A.D., C.D., J.K., F.D.N., M.E., Y.V., and C.M.; structural chemistry analyses, F.D.N. and M.E.; formal analysis, C.T., A.D., G.M.P., M.B., and P.P.; writing – original draft, C.T. and P.P.; writing – review & editing, C.T., A.D., M.E.R., and P.P.; supervision, P.P.

DECLARATION OF INTERESTS

All authors were corporate employees of Firmenich when this work was performed. The work was funded internally, and parts presented herein are covered in the following published patent applications: WO2019122236, WO2019122232, and WO2020127325.

INCLUSION AND DIVERSITY

One or more of the authors of this paper self-identifies as an underrepresented ethnic minority in their field of research or within their geographical location. One or more of the authors of this paper self-identifies as a member of the LGBTQIA+ community.

Received: March 15, 2022
Revised: December 2, 2022
Accepted: March 6, 2023
Published: March 27, 2023

REFERENCES

1. Chess, A., Simon, I., Cedar, H., and Axel, R. (1994). Allelic inactivation regulates olfactory receptor gene expression. Cell *78*, 823–834.
2. Serizawa, S., Miyamichi, K., Nakatani, H., Suzuki, M., Saito, M., Yoshihara, Y., and Sakano, H. (2003). Negative feedback regulation ensures the one receptor-one olfactory neuron rule in mouse. Science *302*, 2088–2094.
3. Khan, M., Vaes, E., and Mombaerts, P. (2011). Regulation of the probability of mouse odorant receptor gene choice. Cell *147*, 907–921.
4. Lyons, D.B., Allen, W.E., Goh, T., Tsai, L., Barnea, G., and Lomvardas, S. (2013). An epigenetic trap stabilizes singular olfactory receptor expression. Cell *154*, 325–336.
5. Malnic, B., Hirono, J., Sato, T., and Buck, L.B. (1999). Combinatorial receptor codes for odors. Cell *96*, 713–723.
6. Araneda, R.C., Kini, A.D., and Firestein, S. (2000). The molecular receptive range of an odorant receptor. Nat. Neurosci. *3*, 1248–1255.
7. Nara, K., Saraiva, L.R., Ye, X., and Buck, L.B. (2011). A large-scale analysis of odor coding in the olfactory epithelium. J. Neurosci. *31*, 9179–9191.
8. Peterlin, Z., Li, Y., Sun, G., Shah, R., Firestein, S., and Ryan, K. (2008). The importance of odorant conformation to the binding and activation of a representative olfactory receptor. Chem. Biol. *15*, 1317–1327.

9. Firestein, S. (2001). How the olfactory system makes sense of scents. Nature *413*, 211–218.
10. Mombaerts, P. (2004). Genes and ligands for odorant, vomeronasal and taste receptors. Nat. Rev. Neurosci. *5*, 263–278.
11. Oka, Y., Omura, M., Kataoka, H., and Touhara, K. (2004). Olfactory receptor antagonism between odorants. EMBO J. *23*, 120–126.
12. Araneda, R.C., Peterlin, Z., Zhang, X., Chesler, A., and Firestein, S. (2004). A pharmacological profile of the aldehyde receptor repertoire in rat olfactory epithelium. J. Physiol. *555*, 743–756.
13. Rioux, D., and Carlson, J.R. (2020). Olfaction: receptor antagonistes. Curr. Biol. *30*, R815–R817.
14. Reddy, G., Zak, J.D., Vergassola, M., and Murthy, V.N. (2018). Antagonism in olfactory receptor neurons and its implications for the perception of odor mixtures. eLife *7*, e34958.
15. Singh, V., Murphy, N.R., Balasubramanian, V., and Mainland, J.D. (2019). Competitive binding predicts nonlinear responses of olfactory receptors to complex mixtures. Proc. Natl. Acad. Sci. USA *116*, 9598–9603.
16. Inagaki, S., Iwata, R., Iwamoto, M., and Imai, T. (2020). Widespread inhibition, antagonism, and synergy in mouse olfactory sensory neurons in vivo. Cell Rep. *31*, 107814.
17. Pfister, P., Smith, B.C., Evans, B.J., Brann, J.H., Trimmer, C., Sheikh, M., Arroyave, R., Reddy, G., Jeong, H.Y., Raps, D.A., et al. (2020). Odorant receptor inhibition is fundamental to odor encoding. Curr. Biol. *30*, 2574–2587.e6.
18. Xu, L., Li, W., Voleti, V., Zou, D.J., Hillman, E.M.C., and Firestein, S. (2020). Widespread receptor-driven modulation in peripheral olfactory coding. Science *368*, eaaz5390.
19. Zak, J.D., Reddy, G., Vergassola, M., and Murthy, V.N. (2020). Antagonistic odor interactions in olfactory sensory neurons are widespread in freely breathing mice. Nat. Commun. *11*, 3350.
20. Leach, K., Sexton, P.M., and Christopoulos, A. (2007). Allosteric GPCR modulators: taking advantage of permissive receptor pharmacology. Trends Pharmacol. Sci. *28*, 382–389.
21. Kenakin, T.P. (2012). Biased signalling and allosteric machines: new vistas and challenges for drug discovery. Br. J. Pharmacol. *165*, 1659–1669.
22. Conn, P.J., Lindsley, C.W., Meiler, J., and Niswender, C.M. (2014). Opportunities and challenges in the discovery of allosteric modulators of GPCRs for treating CNS disorders. Nat. Rev. Drug Discov. *13*, 692–708.
23. Servant, G., Kenakin, T., Zhang, L., Williams, M., and Servant, N. (2020). The function and allosteric control of the human sweet taste receptor. Adv. Pharmacol. *88*, 59–82.
24. Chaput, M.A., El Mountassir, F., Atanasova, B., Thomas-Danguin, T., Le Bon, A.M., Perrut, A., Ferry, B., and Duchamp-Viret, P. (2012). Interactions of odorants with olfactory receptors and receptor neurons match the perceptual dynamics observed for woody and fruity odorant mixtures. Eur. J. Neurosci. *35*, 584–597.
25. Duchamp-Viret, P., Duchamp, A., and Chaput, M.A. (2003). Single olfactory sensory neurons simultaneously integrate the components of an odour mixture. Eur. J. Neurosci. *18*, 2690–2696.
26. Rospars, J.P., Lansky, P., Chaput, M., and Duchamp-Viret, P. (2008). Competitive and noncompetitive odorant interactions in the early neural coding of odorant mixtures. J. Neurosci. *28*, 2659–2666.
27. Rospars, J.P. (2013). Interactions of odorants with olfactory receptors and other preprocessing mechanisms: how complex and difficult to predict? Chem. Senses *38*, 283–287.
28. Gregory, K.J., Sexton, P.M., and Christopoulos, A. (2007). Allosteric modulation of muscarinic acetylcholine receptors. Curr. Neuropharmacol. *5*, 157–167.
29. Gregory, K.J., Sexton, P.M., and Christopoulos, A. (2010). Overview of receptor allosterism. Curr. Protoc. Pharmacol. *Chapter 1*. Unit 1 21.
30. Burford, N.T., Clark, M.J., Wehrman, T.S., Gerritz, S.W., Banks, M., O'Connell, J., Traynor, J.R., and Alt, A. (2013). Discovery of positive allosteric modulators and silent allosteric modulators of the mu-opioid receptor. Proc. Natl. Acad. Sci. USA *110*, 10830–10835.
31. García-Cárceles, J., Decara, J.M., Vázquez-Villa, H., Rodríguez, R., Codesido, E., Cruces, J., Brea, J., Loza, M.I., Alén, F., Botta, J., et al. (2017). A positive allosteric modulator of the serotonin 5-HT2C receptor for obesity. J. Med. Chem. *60*, 9575–9584.
32. Ahn, S., Pani, B., Kahsai, A.W., Olsen, E.K., Husemoen, G., Vestergaard, M., Jin, L., Zhao, S., Wingler, L.M., Rambarat, P.K., et al. (2018). Small-molecule positive allosteric modulators of the beta2-Adrenoceptor isolated from DNA-encoded libraries. Mol. Pharmacol. *94*, 850–861.
33. Stanczyk, M.A., Livingston, K.E., Chang, L., Weinberg, Z.Y., Puthenveedu, M.A., and Traynor, J.R. (2019). The delta-opioid receptor positive allosteric modulator BMS 986187 is a G-protein-biased allosteric agonist. Br. J. Pharmacol. *176*, 1649–1663.
34. Wold, E.A., Chen, J., Cunningham, K.A., and Zhou, J. (2019). Allosteric modulation of Class A GPCRs: targets, agents, and emerging concepts. J. Med. Chem. *62*, 88–127.
35. Kruse, A.C., Li, J., Hu, J., Kobilka, B.K., and Wess, J. (2014). Novel insights into M3 muscarinic acetylcholine receptor physiology and structure. J. Mol. Neurosci. *53*, 316–323.
36. Laing, D.G., and Glemarec, A. (1992). Selective attention and the perceptual analysis of odor mixtures. Physiol. Behav. *52*, 1047–1053.
37. Laing, D.G., and Willcox, M.E. (1987). An investigation of the mechanisms of odor suppression using physical and dichorhinic mixtures. Behav. Brain Res. *26*, 79–87.
38. Miyazawa, T., Gallagher, M., Preti, G., and Wise, P.M. (2008). Synergistic mixture interactions in detection of perithreshold odors by humans. Chem. Senses *33*, 363–369.
39. Wysocki, C.J., Whitney, G., and Tucker, D. (1977). Specific anosmia in the laboratory mouse. Behav. Genet. *7*, 171–188.
40. Whissell-Buechy, D., and Amoore, J.E. (1973). Odour-blindness to musk: simple recessive inheritance. Nature *242*, 271–273.
41. Croy, I., Nordin, S., and Hummel, T. (2014). Olfactory disorders and quality of life–an updated review. Chem. Senses *39*, 185–194.
42. Keller, A., Zhuang, H., Chi, Q., Vosshall, L.B., and Matsunami, H. (2007). Genetic variation in a human odorant receptor alters odour perception. Nature *449*, 468–472.
43. Mainland, J.D., Keller, A., Li, Y.R., Zhou, T., Trimmer, C., Snyder, L.L., Moberly, A.H., Adipietro, K.A., Liu, W.L., Zhuang, H., et al. (2014). The missense of smell: functional variability in the human odorant receptor repertoire. Nat. Neurosci. *17*, 114–120.
44. Trimmer, C., Keller, A., Murphy, N.R., Snyder, L.L., Willer, J.R., Nagai, M.H., Katsanis, N., Vosshall, L.B., Matsunami, H., and Mainland, J.D. (2019). Genetic variation across the human olfactory receptor repertoire alters odor perception. Proc. Natl. Acad. Sci. USA *116*, 9475–9480.
45. Yoshikawa, K., Deguchi, J., Hu, J., Lu, H.Y., and Matsunami, H. (2022). An odorant receptor that senses four classes of musk compounds. Curr. Biol. *32*, 5172–5179.e5.
46. Triller, A., Boulden, E.A., Churchill, A., Hatt, H., Englund, J., Spehr, M., and Sell, C.S. (2008). Odorant-receptor interactions and odor percept: a chemical perspective. Chem. Biodivers. *5*, 862–886.
47. Shirasu, M., Yoshikawa, K., Takai, Y., Nakashima, A., Takeuchi, H., Sakano, H., and Touhara, K. (2014). Olfactory receptor and neural pathway responsible for highly selective sensing of musk odors. Neuron *81*, 165–178.
48. Sato-Akuhara, N., Horio, N., Kato-Namba, A., Yoshikawa, K., Niimura, Y., Ihara, S., Shirasu, M., and Touhara, K. (2016). Ligand specificity and evolution of mammalian musk odor receptors: effect of single receptor deletion on odor detection. J. Neurosci. *36*, 4482–4491.
49. Valant, C., Felder, C.C., Sexton, P.M., and Christopoulos, A. (2012). Probe dependence in the allosteric modulation of a G protein-coupled receptor: implications for detection and validation of allosteric ligand effects. Mol. Pharmacol. *81*, 41–52.

50. Ahmed, L., Zhang, Y., Block, E., Buehl, M., Corr, M.J., Cormanich, R.A., Gundala, S., Matsunami, H., O'Hagan, D., Ozbil, M., et al. (2018). Molecular mechanism of activation of human musk receptors OR5AN1 and OR1A1 by (R)-muscone and diverse other musk-smelling compounds. Proc. Natl. Acad. Sci. USA *115*, E3950–E3958.

51. Hedderich, J.B., Persechino, M., Becker, K., Heydenreich, F.M., Gutermuth, T., Bouvier, M., Bünemann, M., and Kolb, P. (2022). The pocketome of G-protein-coupled receptors reveals previously untargeted allosteric sites. Nat. Commun. *13*, 2567.

52. Launay, G., Téletchéa, S., Wade, F., Pajot-Augy, E., Gibrat, J.F., and Sanz, G. (2012). Automatic modeling of mammalian olfactory receptors and docking of odorants. Protein Eng. Des. Sel. *25*, 377–386.

53. Cometto-Muñiz, J.E., Cain, W.S., and Abraham, M.H. (2003). Quantification of chemical vapors in chemosensory research. Chem. Senses *28*, 467–477.

54. Sato, N., M.S., Kato-Namba, A., Yoshikawa, K., Niimura, Y., Ihara, S., and Touhara, K. (2015). Structure-activity relationship and evolution of musk odor receptors in mammals. Association for chemoreception sciences (AChemS). 37th Annual Meeting Poster #251.

55. Jaeger, S.R., McRae, J.F., Bava, C.M., Beresford, M.K., Hunter, D., Jia, Y., Chheang, S.L., Jin, D., Peng, M., Gamble, J.C., et al. (2013). A Mendelian trait for olfactory sensitivity affects odor experience and food selection. Curr. Biol. *23*, 1601–1605.

56. Li, B., Kamarck, M.L., Peng, Q., Lim, F.L., Keller, A., Smeets, M.A.M., Mainland, J.D., and Wang, S. (2022). From musk to body odor: decoding olfaction through genetic variation. PLoS Genet. *18*, e1009564.

57. Sato-Akuhara, N., Trimmer, C., Keller, A., Niimura, Y., Shirasu, M., Mainland, J.D., and Touhara, K. (2023). Genetic variation in the human olfactory receptor OR5AN1 associates with the perception of musks. Chem. Senses *48*, 9475–9480.

58. Dewan, A., Cichy, A., Zhang, J., Miguel, K., Feinstein, P., Rinberg, D., and Bozza, T. (2018). Single olfactory receptors set odor detection thresholds. Nat. Commun. *9*, 2887.

59. Olender, T., Waszak, S.M., Viavant, M., Khen, M., Ben-Asher, E., Reyes, A., Nativ, N., Wysocki, C.J., Ge, D., and Lancet, D. (2012). Personal receptor repertoires: olfaction as a model. BMC Genomics *13*, 414.

60. Zhou, Q., Yang, D., Wu, M., Guo, Y., Guo, W., Zhong, L., Cai, X., Dai, A., Jang, W., Shakhnovich, E.I., et al. (2019). Common activation mechanism of class A GPCRs. eLife *8*, e50279.

61. Cao, A.M., Quast, R.B., Fatemi, F., Rondard, P., Pin, J.P., and Margeat, E. (2021). Allosteric modulators enhance agonist efficacy by increasing the residence time of a GPCR in the active state. Nat. Commun. *12*, 5426.

62. Virtanen, P., Gommers, R., Oliphant, T.E., Haberland, M., Reddy, T., Cournapeau, D., Burovski, E., Peterson, P., Weckesser, W., Bright, J., et al. (2020). SciPy 1.0: fundamental algorithms for scientific computing in Python. Nat. Methods *17*, 261–272.

63. Vuilleumier, C., Van De Waal, M., Fontannaz, H., Cayeux, I., and Rebetez, P.-A. (2008). Multidimensional visualization of physical and perceptual data leading to a creative approach in fragrance development. Perfumer Flavorist *33*, 54–61.

64. Klein, M.T., Vinson, P.N., and Niswender, C.M. (2013). Approaches for probing allosteric interactions at 7 transmembrane spanning receptors. Prog. Mol. Biol. Transl. Sci. *115*, 1–59.

65. Lawless, H.T. (2010). A simple alternative analysis for threshold data determined by ascending forced-choice methods of limits. J. Sens. Stud. *25*, 332–346.

66. Corcoran, C.D., and Mehta, C.R. (2002). Exact level and power of permutation, bootstrap and asymptotic tests of trend. J. Mod. App. Stat. Meth. *1*, 32–41.

67. Jacobson, M.P., Friesner, R.A., Xiang, Z., and Honig, B. (2002). On the role of the crystal environment in determining protein side-chain conformations. J. Mol. Biol. *320*, 597–608.

68. Jacobson, M.P., Pincus, D.L., Rapp, C.S., Day, T.J., Honig, B., Shaw, D.E., and Friesner, R.A. (2004). A hierarchical approach to all-atom protein loop prediction. Proteins *55*, 351–367.

69. Thompson, J.D., Higgins, D.G., and Gibson, T.J. (1994). Clustal W: improving the sensitivity of progressive multiple sequence alignment through sequence weighting, position-specific gap penalties and weight matrix choice. Nucleic Acids Res. *22*, 4673–4680.

70. Sherman, W., Beard, H.S., and Farid, R. (2006). Use of an induced fit receptor structure in virtual screening. Chem. Biol. Drug Des. *67*, 83–84.

71. Sherman, W., Day, T., Jacobson, M.P., Friesner, R.A., and Farid, R. (2006). Novel procedure for modeling ligand/receptor induced fit effects. J. Med. Chem. *49*, 534–553.

72. Shivakumar, D., Harder, E., Damm, W., Friesner, R.A., and Sherman, W. (2012). Improving the prediction of absolute solvation free energies using the next generation OPLS force field. J. Chem. Theor. Comput. *8*, 2553–2558.

73. Li, J., Abel, R., Zhu, K., Cao, Y., Zhao, S., and Friesner, R.A. (2011). The VSGB 2.0 model: a next generation energy model for high resolution protein structure modeling. Proteins *79*, 2794–2812.

STAR★METHODS

KEY RESOURCES TABLE

REAGENT or RESOURCE	SOURCE	IDENTIFIER
Chemicals, Peptides, and Recombinant Proteins		
DMEM, 1X (Dulbecco's Modification of Eagle's Medium)	Corning	Cat. # 10-013-CM
Fetal Bovine Serum Qualified One Shot	Life Technologies	Cat # A31606-01
HBSS (Hanks' Balanced Salt Solution)	Corning	Cat # 20-023-CV
HEPES (4-(2-hydroxyethyl)-1-piperazineethanesulfonic acid)	Teknova	Cat # H1030
Lipofectamine 2000	Life Technologies	Cat. # 11668
IBMX (3-Isobutyl-1-methylxanthine)	Acros	Cat # 28822-58-4
Propylene glycol	Dow Chemical Company	N/A
Dipropylene glycol	Sigma	Cat # D215554
DMSO (Dimethyl Sulfoxide)	Sigma	Cat # D2438
Critical Commercial Assays		
HTRF cAMP Dynamic 2 Kit	Cisbio	Cat. # 62AM4PEB
Experimental Models: Cell Lines		
HEK293T	ATCC	CRL-3216™
Rtp1 expressing HEK293T	N/A	https://doi.org/10.1016/j.cub.2020.04.086[17]
Experimental Models: Organisms/Strains		
Human subjects	N/A	N/A
Recombinant DNA		
pPUR Vector	Clontech	Cat. # 631601
pGEM®-T Easy Vector	Promega	Cat. # A1360
Software and Algorithms		
Prism 8.1.2	GraphPad	https://www.graphpad.com/scientific-software/prism/
RStudio	Foundation for Open Access Statistics	https://www.rstudio.com/
Inkscape 0.92.3	Inkscape Project	https://inkscape.org/
BioEdit 7.2.6	BioEdit	https://bioedit.software.informer.com/
SciPy 1.7.3	https://scipy.org/	https://doi.org/10.1038/s41592-019-0686-2[62]
Induced Fit Docking	Schrödinger	https://www.schrodinger.com/products/ifd-md

RESOURCE AVAILABILITY

Lead contact

Further information and requests for resources and reagents should be directed to and will be fulfilled by the lead contact, Patrick Pfister (patrick.pfister@firmenich.com).

Materials availability

- Volatile compounds were sourced internally, all other reagents are commercially available (see key resources table).
- An Rtp1-expressing HEK293T cell line was used. There are restrictions to the availability of this cell line due to existing intellectual property (WO2016201153A1).

Data and code availability

- The data that support the findings of this study are given in Tables S1–S3.

- Additional data are available from the lead contact upon reasonable request.
- The code used for analysis and figure generation is disclosed and referenced. No original code is reported.

EXPERIMENTAL MODEL AND SUBJECT DETAILS

Human Subjects

A total of 115 subjects participated in the study. Each subject gave informed consent and was financially compensated for their time and effort. Exclusion criteria for participation were pregnancy, nursing, allergy or sensitivity to fragrances or food, asthma, acute or chronic impairments of olfaction, and being younger than 17 or older than 65 years of age.

METHOD DETAILS

Odor detection thresholds determination

Determination of group odor detection thresholds (gODT)

The determination of dose-response relationship and group odor detection threshold were combined in an iterative process and fully described.[63] Briefly, air-dilution olfactometers allow for controlled and precise gas phase concentration delivery of test chemicals. Odorants were diluted in mixtures of propylene glycol (PG) and dipropylene glycol (DiPG) and injected into a heated flask (130°C) under a nitrogen stream (60L/h) resulting in forced evaporation and accurate concentrations. Humidified air (540 L/h and 50% Relative Humidity at 27°C) was used to dilute this primary flow. Test compounds were evaluated by a set of 30-40 panelists. First, a dose-response relationship is determined between perceived intensities over a range of concentrations. Panelists evaluate 4 concentrations of the ingredient, regularly spaced on a logarithmic scale between 10^{-6} μg/l air and its volatility. Depending on the results, 4 additional concentrations are tested to complete the curve. Sigmoidal data treatment leads to the expression of the averaged intensity versus gas phase concentration. Group odor detection threshold are then evaluated by three-alternative forced-choice (3-AFC) tests. Panelists evaluated 3 concentrations at low intensities in the dose-response relationship previously established. 3 additional concentrations were evaluated to complete the dataset. A sigmoidal data treatment supports the expression of the percentage of correct choice versus gas phase concentration. Group odor detection threshold was set at the gas phase concentration corresponding to 66.6% of correct choices (i.e. 50% of the subjects made the correct choice).

Determination of individual odor detection thresholds (iODT)

Individual odor detection thresholds were measured for a group of about 60 subjects using a modified Up and Down procedure. gODT established represent the starting point for the concentrations range to be evaluated. Measurements were based on successive individual evaluations of paired samples (odor vs blank). Correct or incorrect choice between odor and blank determined the decrease or increase of the odor concentration of the next sample pair. Binary dilutions steps were used and result in a "sensory walk" for the subjects. After 5 consecutive inversions (errors), the individual odor detection threshold was calculated as the geometric mean from the 4 last inversion concentrations. If the subject sensitivity appeared to be out of the initial concentration range, complementary sessions were organized. The Spearman correlation matrix was generated using the iODT values for each musk.

Homogeneous time resolved fluorescence (HTRF) assay and high-throughput screening

All OR genes were generated, expressed and their activity assayed as previously described.[17] Enhancement dose-response experiments were obtained by mixing each agonist test concentration with a single concentration of the putative enhancing compound. To maintain the solvent concentration constant across the assay plate and minimize solubilization limitations, binary mixture stock solutions were first made in 100% dimethyl sulfoxide prior to a dilution step to reach the final test concentrations (final DMSO concentration = 0.1%). The same conditions were used for the high-throughput screening of putative enhancing compounds. A library of 780 odorants sourced internally was assembled in 100% solvent (DMSO) at a stock concentration of 300 mM and stored at -20°C. Compounds were diluted to a final concentration of 300 μM (final DMSO concentration = 0.1%) in a 96 well plate format and delivered to cells transfected with the Flag-Rho tagged human OR5AN1 sequence for screening. Lucy-Flag-Rho OR5AN1 was used for Schild experiments. Point mutations to assess allosteric binding were generated in the background of allele 289F. Categorization between inhibiting, neutral and activating/enhancing compounds was performed on a per plate basis and 3 standard deviation from the mean base line. Enhancement was assessed by measuring the change in receptor activation elicited by 300 μM of each compound in the presence of an EC_{20} concentration of muscenone® delta, allowing for a large assay window to identify OR5AN1 activity beyond 20% efficacy.[64]

Allosteric modulation parameter calculations

Dose-response data were analyzed and graphed in GraphPad Prism 8.1.2. The standard errors of the mean were calculated for duplicate conditions. Agonist data points were fitted to a four parameter non-linear regression following the Hill equation (unconstrained Hill coefficient) to calculate EC_{50}, Hill coefficient, maxima and minima of the response signals. To determine the parameters of the modulatory effect observed, data points for binary mixtures were fitted to the operational allosteric model[20,21]:

$$Response = \frac{\tau_A[A]/K_A(1+\alpha\beta[B]/K_B)+\tau_B[B]/K_B}{[A]/K_A\{(1+\alpha[B]/K_B)+\tau_A(1+\alpha\beta[B]/K_B)\}+[B]/K_B(1+\tau_B)+1}$$

Where [A] is the concentration of the agonist; [B] is the concentration of the allosteric modulator; K_A and K_B are the equilibrium dissociation constants of the agonist and the modulator, respectively; α is the cooperativity factor that governs the potency magnitude and direction of the allosteric modulation when the two ligands both occupy the receptor. Negative potency modulation occurs when $0 < \alpha < 1$; positive potency modulation occurs when $\alpha > 1$. β is the cooperativity factor that governs the efficacy magnitude and direction of the allosteric modulation when the two ligands both occupy the receptor. Negative efficacy modulation occurs when $0 < \beta < 1$ and positive efficacy modulation occurs when $\beta > 1$. T_A and T_B are the intrinsic efficacies of the agonist and the modulator, respectively. Model fitting was performed using custom written Python code to implement robust regression with the SciPy package.[62] The dose response curves were first normalized to 40% of the maximum agonist response acquired on the same day. Mutant receptors were normalized to the corresponding wildtype receptor response. To ensure biologically plausible values, model parameters were constrained as follows: $0 < T_A < 1$, $0 < T_B < 1.2$, $10\text{-}9 < K_A < 0.01$, $10\text{-}9 < K_B < 0.1$, $0 < \alpha < 100$, $0 < \beta < 100$. Model fits were evaluated with visual inspection as well as by calculating RMSE, which averaged 0.04 across all models.

Psychophysical assessment of enhancement

Pre-testing

We first measured dose-response functions for all four aldehyde odorants ((E)-2-tridecenal, (Z)-4-dodecenal, (Z)-2-nonenal, and nonanal) to ensure their iso-intensity for ODT sessions (see below). The odorant dilutions, prepared weight/weight percent in DiPG, were a series of eight concentrations spanning the range from 0.0032% to 100%. To ascertain reliability, the third-lowest concentration was duplicated in each session. Test samples were 16 oz. glass jars with plastic flip-top lids, containing two paper souffle dishes with a cellulose pad in each dish. One cellulose pad was dosed with 250μl of odorant dilution. The other cellulose pad was dosed with 250μL of DiPG. Samples were equilibrated for 2 hours and used 2-4 hours after being dosed.

During the dose-response session, eight blind-coded samples (six concentrations, one duplicate and one 'blank' (DiPG)) with the same odorant were presented in a randomized order that was counterbalanced across subjects. Subjects rated the intensity of the sample on a 0-10 line scale, with a 1min inter-stimulus interval. A dose-response curve was obtained by fitting a 2-parameter logistic model.

Next, to ensure their iso-intensity, concentrations corresponding to the intensity of 5 (based on the dose-response curves) of all four aldehydes were rated on intensity by panelists within the same session.

ODT sessions

To obtain reliable odor detection data for muscenone® delta, 50 ODT sessions (11 sessions for the (Z)-2-nonenal condition, and 13 sessions each for (E)-2-tridecenal, nonanal, and (Z)-4-dodecenal) were conducted, with most subjects participating in multiple sessions; for (R)-(-)-muscone (muscone laevo), 28 ODT sessions (14 sessions each for (Z)-2-nonenal and nonanal) were conducted, with most subjects participating in multiple sessions. Enhancer versus neutral conditions were randomly interspersed over time and were similar in terms of subject demographics in each condition.

The methods used to measure the ODT functions of the target odorant (muscenone® delta or muscone) in the context of enhancement differed from the ones used in the gODT experiments in several respects. First, due to resource constraints, odorants were presented in jars rather than an olfactometer in a 3-AFC task. Second, each challenge of the task required the participant to detect the target odorant against the background of another odorant (enhancer or control depending on experimental condition). Namely, each challenge involved a set of three blind-coded jars, one of which contained one pad dosed with 250 μL of aldehyde dilution and one pad dosed with 250 μL of the ligand (muscenone® delta or muscone depending on the study) dilution in DiPG; the other two jars contained one pad with 250 μL of aldehyde dilution and one pad with 250 μL of DiPG. In other words, for each aldehyde, the concentration determined to be iso-intense from the pre-tests was used in all three jars. After evaluating the three samples in a randomized order that was counterbalanced across subjects, participants selected the odd sample in the set. Starting with the set containing the lowest ligand concentration, each subject progressed to the set with the next highest concentration and so on. There was a 1min inter-stimulus interval between sets. While no more than six ligand concentrations were included in a given test session, repeated ODT sessions enabled us to quantify detection at eight different ligand concentrations, ranging from 13.81E-05M to 4.31M (for muscenone® delta) or from 42.78E-05M to 4.28M (for muscone laevo). In all other respects, the methods followed the ASTM E679 standard (2008) that is commonly used for determining odor and taste thresholds.

Data analysis

To compute detection probabilities, percent correct for each ligand concentration was averaged across sessions and corrected for the probability of guessing.[65] Separately for each condition, the detection probabilities were fit with a 3-parameter logistic model (see Results). To compute 95% confidence intervals (CI's) around each parameter, this procedure was bootstrapped using 10,000 repetitions. To calculate the exact *p*-values, randomization tests[66] involving 10,000 repetitions were applied to build a null-hypothesis distribution for each difference of interest.

Homology modeling and docking of OR5AN1

Following the procedure in Ahmed et al.,[50] we built the homology model of OR5AN1 using Prime in the Schrodinger Suite[67,68] based on the M2 muscarinic acetylcholine receptor (PDB ID: 3UON) as a template. OR5AN1 and template sequences were aligned using

CLUSTAL W,[69] followed by manual adjustments to match the alignment shown in the reference. Molecular docking and calculation of the binding free energy of modulators to the homology model was performed by applying the Induced Fit Docking (IDF) protocol in the Schrodinger Suite.[70,71] A grid box was set with 12Å dimension from the centroid on the receptor residues Phe32 and Lys81. The H-bond constraint was applied to Lys81 so that the ligands interact with the NH2 group of the Lys81 side chain. The ligand binding free energy was estimated by the molecular mechanics energies combined with the generalized Born and surface area continuum solvation (MM-GBSA) method using the OPLS force field[72] and the implicit solvent model VSGB.[73]

QUANTIFICATION AND STATISTICAL ANALYSIS

Compounds in single-concentration screening for possible enhancers were determined to have increased or decreased OR5AN1 response to muscenone® delta if the response was greater than 3 standard deviations above or below the baseline response, as described in Figure 2A. The distribution of fold-change in potency and efficacy was described by mean and standard error of the mean, as seen in Figure 3A. The number of times each potential enhancer was tested ranged between 1 and 19 times. The top nine enhancers were tested on average 6 times.

Dose-response data was described by mean and standard error of the mean of the experiments, with the number of times the assay was performed stated in the figure legends, if greater than once.

All individual model fits for the allosteric model can be found in Table S2. For each of these fits, the RMSE was calculated for the model to assess model fit. Summary data for these fits is described in Table S3. Here, the number of each repeated experiment (ranging from 2 to 12) is listed as well as the median and interquartile range to describe center and dispersion of the fit parameters across repeated experiments. When comparing the allosteric fits of receptors mutated at different residues, the center and spread of the distribution was described in boxplots with the median and interquartile range, as seen in Figure 5A. The whiskers denote the estimate edges of the distribution, as computed by 1.5 times the interquartile range subtracted from the first quartile. The Mann-Whitney U test was used to assess significance when comparing parameters of fits to the mutant receptors, as listed in the results.

Statistical analyses of data from human subjects are described in legends to Figures 1 and 6 and were based on the alpha level of 0.05. To obtain dose-response curves for the four aldehyde compounds, the following 2-parameter logistic model was fit to the intensity ratings: $Y = 10/(1+e^{-h*(\log(x) - \theta)})$, where X is molar concentration of an aldehyde, Y is rated intensity on a scale of 0 to 10, h is the Hill coefficient, and θ is molar concentration associated with the intensity of 5.

To model detection probabilities as a function of musk concentration, the following 3-parameter logistic model was fit to mean detection probabilities at each concentration: $Pd = (\text{Max Pd})/(1+e^{-h*(\log(x) - \theta)})$, where X is molar concentration of a musk, Pd is mean probability of detection at a given concentration, Max Pd is asymptotic probability of detection with increasing concentration, h is the Hill coefficient, and θ is molar concentration at which the probability of detection equals Max Pd/2.

For statistical comparisons of ODT curves, bootstrapping and randomization tests in RStudio were used to compute 95% confidence intervals around each curve parameter of interest (see legend to Figure 6) and calculate the exact p-values for each contrast of interest, respectively. These nonparametric methods do not rely on the assumptions of normality and homogeneity of variance.